

The Activation of DNA Damage Detection and Repair Responses in Cleavage-Stage Rat Embryos by a Damaged Paternal Genome

Lisanne Grenier,* Bernard Robaire,*† and Barbara F. Hales*¹

*Department of Pharmacology and Therapeutics; and †Department of Obstetrics and Gynecology, McGill University, Montreal, Quebec H3G 1Y6, Canada

¹To whom correspondence should be addressed. Fax: (514) 398-7120. E-mail: barbara.hales@mcgill.ca.

Received January 24, 2012; accepted March 12, 2012

Male germ cell DNA damage, after exposure to radiation, exogenous chemicals, or chemotherapeutic agents, is a major cause of male infertility. DNA-damaged spermatozoa can fertilize oocytes; this is of concern because there is limited information on the capacity of early embryos to repair a damaged male genome or on the fate of these embryos if repair is inadequate. We hypothesized that the early activation of DNA damage response in the early embryo is a critical determinant of its fate. The objective of this study was to assess the DNA damage response and mitochondrial function as a measure of the energy supply for DNA repair and general health in cleavage-stage embryos sired by males chronically exposed to an anticancer alkylating agent, cyclophosphamide. Male rats were treated with saline or cyclophosphamide (6 mg/kg/day) for 4 weeks and mated to naturally cycling females. Pronuclear two- and eight-cell embryos were collected for immunofluorescence analysis of mitochondrial function and biomarkers of the DNA damage response: γ H2AX foci, 53BP1 reactivity, and poly(ADP-ribose) polymer formation. Mitochondrial activities did not differ between embryos sired by control- and cyclophosphamide-exposed males. At the two-cell stage, there was no treatment-related increase in DNA double-strand breaks; by the eight-cell stage, a significant increase was noted, as indicated by increased medium and large γ H2AX foci. This was accompanied by a dampened DNA repair response, detected as a decrease in the nuclear intensity of poly(ADP-ribose) polymers. The micronuclei formed in cyclophosphamide-sired embryos contained large γ H2AX foci and enhanced poly(ADP-ribose) polymer and 53BP1 reactivity compared with their nuclear counterparts. Thus, paternal cyclophosphamide exposure activated a DNA damage response in cleavage-stage embryos. Furthermore, this damage response may be useful in assessing embryo quality and developmental competence.

Key Words: cyclophosphamide; γ H2AX; 53BP1; poly(ADP-ribose) polymers; spermatozoa; embryo; epigenetic marks.

Millions of men of reproductive age now survive cancer as a consequence of improvements in cancer treatment regimens consisting of chemotherapeutic agents and/or radiation (Green *et al.*, 2010). However, fertility is of concern to many of these men because these treatment regimens usually lead to an initial

drop in sperm production that may be sustained for months to years, causing infertility in a large proportion of subjects (Green *et al.*, 2010). Even men who recover spermatogenesis may still be infertile and may be faced with the possibility of transmitting heritable genetic diseases to their offspring. Cyclophosphamide, a nitrogen mustard compound, is commonly used as a cancer therapeutic and immunosuppressant agent. This drug is a bifunctional alkylating agent, forming DNA adducts, DNA cross-links, and single and double-strand DNA breaks in dividing cells. The exposure of male rats to cyclophosphamide induces DNA damage in spermatozoa that ranges from DNA double-strand breaks (DSBs) and single-strand breaks to chromosomal aberrations (Barton *et al.*, 2003; Codrington *et al.*, 2004). Furthermore, this paternal cyclophosphamide treatment results in dose-dependent and time-specific effects on progeny outcome, including pre- and postimplantation loss, malformations, and deficits in learning behavior; some of these outcomes are observed in subsequent generations (Auroux *et al.*, 1990; Hales *et al.*, 1992; Trasler *et al.*, 1986). Our labs, and others, have used cyclophosphamide to elucidate the mechanisms underlying male-mediated developmental toxicity (Barton *et al.*, 2007; Grenier *et al.*, 2011).

The male genome is tightly packaged for delivery to the oocyte (Ward, 2010); paternal drug exposures may disturb the packaging of male germ cell chromatin. Indeed, paternal cyclophosphamide treatment alters the sperm basic proteome, and specifically, some components of the nuclear matrix that may be involved in events during spermiogenesis and fertilization (Codrington *et al.*, 2007a,b). The timing of spermatozoal decondensation and the deposition of modified histones are accelerated in zygotes fertilized by spermatozoa from cyclophosphamide-treated males (Grenier *et al.*, 2010). In pronuclear-stage embryos sired by drug-treated males, the epigenetic programming of both parental genomes is disrupted, as manifested by changes in the regulation of histone H4 acetylation at lysine 5 and in DNA methylation (Barton *et al.*, 2005). The incidence of micronuclei is dramatically elevated in two-cell embryos fertilized by spermatozoa from cyclophosphamide-treated fathers; moreover, the presence of these

micronuclei is associated with developmental delay (Grenier *et al.*, 2011) and is reflected by the proportion of peri-implantation embryonic loss observed in previous studies (Trasler *et al.*, 1986). Together, these findings demonstrate that paternal exposure to cyclophosphamide damages the male genome and disrupts postfertilization events in the early embryo.

Functional mitochondria are crucial for fertilization and determine the developmental potential of early embryos. Stage-specific changes in the functional compartmentalization of mitochondria are required to meet the energy needs of embryos throughout preimplantation development (van Blerkom, 2011). Furthermore, the activation and maintenance of DNA damage responses require the energy produced by mitochondria.

There are multiple DNA damage and repair pathways in cells. DNA damage, in the form of DSBs, is detected by the rapid phosphorylation of histone H2AX at serine 139 (Rogakou *et al.*, 1998). Small γ H2AX foci are associated with cell-cycle regulation and mitosis, medium foci ($0.30\text{--}9.99\ \mu\text{m}^3$) act as repair platforms, recruiting DNA repair proteins to sites of damage, and large foci are indicative of DNA damage accumulation and DNA DSB aggregates (McManus and Hendzel, 2005; Paull *et al.*, 2000). γ H2AX foci are induced in the male pronuclei of zygotes sired by cyclophosphamide-treated male rats (Barton *et al.*, 2007; Grenier *et al.*, 2010).

Large γ H2AX foci colocalize with DNA DSB repair proteins (McManus and Hendzel, 2005), including p53-binding protein 1 (53BP1) and poly(ADP-ribose) polymerase-1 (PARP-1) (Paull *et al.*, 2000). 53BP1, a component of the nonhomologous end joining repair pathway, is involved in DNA damage-induced cell cycle arrest and participates in DNA repair (Wang *et al.*, 2002; Ward *et al.*, 2003). In somatic cells, 53BP1 displays both cytoplasmic and nuclear localizations (Iwabuchi *et al.*, 1998). Inhibition of the nuclear importation of 53BP1 decreases ionizing radiation-induced 53BP1 focus formation, delays DNA repair, and impairs cell survival (Moudry *et al.*, 2011). In the early mouse zygote, 53BP1 is present only in the cytoplasm, whereas by the late pronuclear stage, some staining is found in the pronuclei (Ziegler-Birling *et al.*, 2009). In the two- and eight-cell stages, staining is enriched in the nuclei, but no particular association is observed with any nuclear structure.

Poly(ADP-ribose) (PAR) polymerase-1 (PARP-1) is activated by DNA single-strand breaks and at stalled replication forks to facilitate DNA repair. In response to DNA damage, PARP-1 catalyzes the formation of poly(ADP-ribose) (PAR) polymers, with nicotinamide adenine dinucleotide (NADH) as an energy cofactor, covalently modifying acceptor structural chromatin proteins (Schreiber *et al.*, 2006) and decondensing the chromatin to allow access of other repair factors to sites of DNA damage (Zhou *et al.*, 2010). The removal of PAR polymers is primarily catalyzed by PAR glycohydrolase (PARG) (Brochu *et al.*, 1994). The metabolism of PAR is important during chromatin dynamics, DNA replication, and

repair (D'Amours *et al.*, 1999; Kim *et al.*, 2004). The proper regulation of PARP-1 is critical for the maintenance of genomic stability (Schreiber *et al.*, 2006) because PARP-1 functions as a DNA repair protein in response to single-strand breaks, in the base excision repair pathway (Dantzer *et al.*, 1999), and in the induction of cell death in response to genotoxic stress (Yu *et al.*, 2002). Interestingly, in pronuclear-stage zygotes sired by cyclophosphamide-treated males, PARP-1 immunoreactivity is substantially elevated, not only in the damaged paternal genome but also in the maternal genome (Barton *et al.*, 2007).

The genetic disruption of maternal DNA DSB repair in mice significantly increased the frequency of zygotes with chromosomal structural aberrations after paternal exposure to ionizing radiation (Marchetti *et al.*, 2007). Thus, DNA damage detection and repair responses play an important role in determining progeny outcome. The first goal of these studies was to elucidate the impact of a damaged male genome on mitochondrial bioenergetics and DNA damage detection and repair responses in the cleavage-stage embryo. The second goal was to determine the impact of the formation of micronuclei and of developmental delay in the cleavage-stage embryos on their capacity to mount appropriate DNA damage responses.

MATERIALS AND METHODS

Animals, drug treatment, and embryo collection. This study was done in accordance with the guidelines of the Canadian Council on Animal Care for the ethical use and care of animals in science. The animal treatment protocol (Protocol Number: 2144) was approved by the Animal Care Committee of McGill University.

Adult male (350–400 g) and virgin female (225–250 g) Sprague Dawley rats were purchased from Charles River Canada (St Constant, Quebec, Canada) and housed at the Animal Resources Centre, McIntyre Medical Building, McGill University (Montreal, Canada). Animals received food and water *ad libitum* and were maintained on a 0700 h–1900 h light/dark cycle. The drug treatment and zygote protocols previously described (Grenier *et al.*, 2011; Trasler *et al.*, 1986) were followed with minor modifications. After 1 week of acclimatization, male rats were randomly assigned to one of two treatment groups and gavaged with saline (SAL, vehicle control) or cyclophosphamide (CAS 6055-19-2; Sigma Chemical Co., St Louis, Missouri), 6 mg/kg/day, six times per week for 4 weeks.

On the fifth week of treatment, control virgin females in proestrus (as assessed by a vaginal wash in mid-afternoon) were caged overnight in groups of two with either a control- or cyclophosphamide-treated male. Pregnancies were confirmed with sperm-positive vaginal smears the following morning, designated as gestation day 0. Sperm-positive females were euthanized on day 0 at 1300 h, on day 1 at 1000 h, and day 3 at 1000 h to collect pronuclear zygotes, 2-cell and 8- to 16-cell embryos, respectively. Oviducts and whole uteri were isolated and cleaned in prewarmed (37°C) M2 culture medium (Sigma Chemical Co.); pronuclear zygotes were collected from the ampullae in warm M2 medium, and early cell cleavage embryos were flushed with a 30 round gauge needle from the infundibulum of the oviduct with 0.2 ml of warm M2 medium.

Detection of mitochondrial activity in cleavage-stage embryos. Functional mitochondria were visualized in cleavage-stage embryos using MitoTracker Green FM (catalog number M7514; Invitrogen, Burlington, Ontario, Canada) and MitoSox Red mitochondrial superoxide indicator (catalog number M36008; Invitrogen) probes. Embryos were incubated *in vitro* in

modified rat 1-cell embryo culture medium (mR1ECM) milieu (Oh *et al.*, 1998). Final concentrations of 100nM for MitoTracker Green FM and of 2 μ M for MitoSox Red were prepared in mR1ECM plus bovine serum albumin (BSA, 4.0 mg/ml; pH equilibrated to 7.4 with 12N HCl). This zygotic development milieu was covered with light mineral oil to prevent evaporation and pre-equilibrated for 3 h before incubation at 37°C and 5% CO₂. All solutions and dilutions were prepared fresh the day of the experiment.

Sperm-positive females were euthanized at 1000 h on days 1 and 3 to collect two- and eight-cell embryos in prewarmed (37°C) M2 culture medium (Sigma Chemical Co.). Embryos were flushed with prewarmed (37°C) M2 medium, washed three times in prewarmed (37°C) mR1ECM plus BSA, and incubated in pre-equilibrated (37°C and 5% CO₂) mR1ECM plus BSA with either 100nM MitoTracker Green FM or 2 μ M MitoSox Red. The time from embryo collection to the *in vitro* incubation was completed in less than 7 min to preserve embryo quality. Live *in vitro* embryos were incubated with MitoTracker probes for 20 min to allow the accumulation of the probes in active respiring mitochondria. For the immunodetection of MitoTracker mitochondrion-selective probes, the same immunofluorescence protocols were used as previously described for the Invitrogen molecular probes under the experimental protocol requiring fixation and permeabilization after staining with minor changes. Fixed and permeabilized embryos were incubated for 1 h in goat blocking solution (10% goat serum, 3% BSA, and 0.1% Tween 20 in PBS), and DNA was then stained with 4',6-diamidino-2-phenylindole, dihydrochloride (DAPI), 10 μ g/ml, diluted in goat blocking solution, for 20 min. Embryos were then washed in 0.05% Tween 20 in PBS for 10 min and mounted in 3 μ l of VectaShield mounting medium (Vector Laboratories) on a premarked pap pen slide and covered with a cover slip. Slides were then stored at 4°C and visualized with confocal microscopy within 2 days.

Immunofluorescence detection of markers of DNA damage and repair. The immunofluorescence protocols used were described previously (Grenier *et al.*, 2010). To characterize DNA damage responses, cleavage-stage embryos were incubated with mouse monoclonal IgG anti- γ H2AX phosphoserine 139 (clone JBW103, 1:100 dilution; catalog number 05-636, Upstate Biotechnology, Charlottesville, VA) for 1 h at 37°C, rabbit polyclonal anti-53BP1 (1:100 dilution; catalog number NB100-304, Novus Biological, Oakville, Ontario, Canada), or rabbit polyclonal anti-Poly (ADP-Ribose) (PAR) (1:100 dilution; catalog number 51-8114KC, BD Bioscience Pharmingen, Mississauga, Ontario, Canada) overnight at 4°C in a humidified chamber. Both primary and secondary antibodies were diluted in goat blocking solution (10% goat serum, 3% BSA, and 0.1% Tween 20 in PBS). Zygotes were then washed 3 \times 15 min in goat blocking solution, incubated for 1 h at room temperature with the secondary antibody, goat fluorescein anti-mouse IgG (fluorescein isothiocyanate) (1:100 dilution; catalog number ab97022, Abcam, Cambridge, MA) and goat fluorescein anti-rabbit IgG (H+L) (1:200 dilution; catalog number F1-1000, Vector Laboratories, Burlington, Ontario, Canada), and re-washed 3 \times 15 min in goat blocking solution. DNA was stained with propidium iodide (catalog number P4864; Sigma Chemical Co.) at 10 μ g/ml in goat blocking solution for 20 min, washed in 0.05% Tween 20 in PBS for 10 min and mounted in 3 μ l of VectaShield mounting medium (Vector Laboratories) on a premarked pap pen slide and covered with a cover slip. Slides were then stored at 4°C and visualized with confocal microscopy within 2 days.

Confocal microscopy. A Zeiss LSM 510 Axiovert 100M confocal microscope with a Plan-Apochromat \times 63/1.4 oil differential interference contrast objective was used to visualize the fluorescence of early cleavage-stage embryos. The best settings for laser scanning fluorescence imaging were determined experimentally for all primary antibodies and maintained for all cell cleavage-stage embryos. All embryos were scanned at a speed of 5–7 with an optical slice of 0.6 μ m, zoom factor equal to 1, and a pinhole setting of 96 μ m. Two scans of each optical section were compiled and averaged by the Zeiss LSM 510 computer software to give a final image that was 1024 \times 1024 pixels in size. The embryonic cell cleavage stage was determined by counting the number of nuclei stained with propidium iodide or DAPI and confirmed with phase-contrast images. The presence of micronuclei as nuclear entities detached

from the main nucleus in an embryo was determined with the nuclear propidium iodide stain or DAPI. In addition, the nuclei of blastomeres containing micronuclei were identified using the phase-contrast images. The γ H2AX, 53BP1, PAR, and MitoSox embryo immunofluorescence images from Z-stacks were further analyzed and quantified using the Imaris image analysis program version 7.2.3 (Bitplane, Inc., South Windsor, CT).

Quantitative Analysis. The unit of measure (N) was the number of males; the number of embryos that are indicated below was the average number per male. Quantification of mitochondrial activity was done using the MitoSox probe because the quality of the images with this probe was superior to those obtained with MitoTracker Green; at the two- and eight-cell stages, $N = 5$ control males, with 28 and 41 embryos, and $N = 6$ cyclophosphamide-treated males, with 32 and 39 embryos, respectively, were analyzed. We analyzed all mitochondria above a set minimum threshold intensity; the mitochondrial MitoSox intensity means and counts of all mitochondria were compared in control- and cyclophosphamide-sired embryos from each cleavage stage.

Immunofluorescence z-stack images were used to quantify γ H2AX foci per nucleus in two- and eight-cell embryos sired by control- and cyclophosphamide-treated males and in the micronuclei found in embryos sired by cyclophosphamide-treated males. For the control group, $N = 7$ males with 64 embryos and $N = 10$ males with 99 embryos were analyzed at the two- and eight-cell stage, respectively, and in the cyclophosphamide-sired embryo group, $N = 5$ males with 56 embryos and $N = 7$ males with 112 embryos were analyzed at the two- and eight-cell stage, respectively. For the analysis of 53BP1 reactivity, at the pronuclear, two- and eight-cell stages in the control group, the sample size was $N = 6$ males with 58 embryos, $N = 8$ males with 57 embryos, and $N = 7$ males with 63 embryos, respectively; in the cyclophosphamide-treated group, there were $N = 5$ males with 39 embryos, $N = 4$ males with 32 embryos, and $N = 7$ males with 68 embryos analyzed. PAR polymers were quantified in pronuclear zygotes, two- and eight-cell embryos: in controls, sample sizes of $N = 6$ males with 51 embryos, $N = 7$ males with 58 embryos, and $N = 8$ males with 72 embryos, respectively, were studied; in the cyclophosphamide-treated group, a sample size of $N = 4$ males with 45 embryos, $N = 5$ males with 34 embryos, and $N = 6$ males with 52 embryos was analyzed at each cleavage stage, respectively. The chromatin structure in nuclei was compared at the two- and eight-cell stages to that in micronuclei in cyclophosphamide-sired embryos, using $N = 5$ and 7 males with 41 and 112 embryos for γ H2AX analysis, $N = 4$ and 6 males with 24 and 45 embryos for 53BP1, and $N = 5$ and 6 males with 23 and 37 embryos for PAR detection, respectively.

Measurements relevant to our hypothesis and specific for each DNA damage response marker were analyzed using Imaris (Bitplane Inc.). In our analysis of DNA damage with γ H2AX as a marker, a nuclear surface was created from propidium iodide staining for each embryo to measure the average nuclear and micronuclear volume; within that surface, the total number of nuclear and micronuclear γ H2AX foci were quantified based on their volume: small foci, 0–0.29 μ m³; medium foci, 0.30–9.99 μ m³; or large foci, 10 μ m³ and above. The data were graphed as the average number of γ H2AX foci per nucleus on each embryo collection day. To compare the DNA damage in nuclei to that in micronuclei, the nuclear value was set to 1, and the fold difference between the micronuclei and nuclei was examined; all values were corrected for nuclear and micronuclear volume.

The 53BP1 and PAR average nuclear and micronuclear intensity means were assessed relative to the DNA intensity assessed based on the nuclear surface created from propidium iodide staining for each embryo. A second surface was created inversely from propidium iodide staining to capture all the cytoplasmic staining to measure the average intensity mean of 53BP1 and PAR immunofluorescence in the cytoplasm. To characterize the micronuclear chromatin content of these DNA repair indicators, data were graphed as the 53BP1 and PAR fold difference from nuclear average intensity, comparing the micronuclear to nuclear ratios; the 53BP1 and PAR intensity ratio are relative to the micronuclear to nuclear DNA intensity ratio, set at 1 to correct for the difference in DNA intensity.

Statistical analyses. All statistical analyses were done using Systat (program version 10.2, Chicago, IL). Kruskal-Wallis analysis was done to analyze for the drug effect between control- and cyclophosphamide-sired embryos with respect to 53BP1 and PAR nuclear and cytoplasmic staining and nuclear to cytoplasmic intensity mean ratios at each cleavage stage. Kruskal-Wallis analysis, with Bonferroni's correction when needed, was done to determine a time effect between cleavage stages within a treatment group on the 53BP1 and PAR nuclear, cytoplasmic, and the nuclear to cytoplasmic intensity mean ratios.

Mann-Whitney *U*-test was used to assess any differences in the number of γ H2AX foci between treatment groups at a specific cleavage stage and between cleavage stages within a treatment group. We also used the Mann-Whitney *U*-test to assess the difference in the micronuclear and nuclear chromatin structure for γ H2AX, 53BP1, and PAR immunoreactivity, as well as the average numbers of small, medium, and large γ H2AX foci per micronucleus (corrected for volume) between cleavage stages. Values are reported either as an average number of foci or intensity mean per embryo per replicate \pm SEM or fold difference from the nuclear number of foci or micronuclear to nuclear DNA intensity means, set to $1 \pm$ SEM.

RESULTS

Mitochondrial Function

Because mitochondrial activity is a useful measure of embryo quality, we monitored their localization, numbers, and activity within each blastomere of live cleavage-stage embryos using MitoTracker green and MitoSox red probes (Fig. 1). These fluorescent mitochondrial probes are selective indicators of mitochondrial function and energy production. In addition, MitoSox red provides a measure of oxidative stress because it indicates the presence of superoxide generated as a byproduct of oxidative phosphorylation by a leaky mitochondrial electron transport chain during adenosine triphos-

phate (ATP) production. We obtained similar mitochondrial staining patterns with both MitoTracker probes, but for stability, reproducibility, and image quality reasons, the data analysis was focused on the MitoSox red probe. As anticipated, the mitochondrial staining pattern was excluded from the nucleus in all cleavage-stage embryos. In two- to four-cell embryos, we detected the presence of numerous bean shape mitochondria distributed throughout each individual blastomere (Fig. 1a). Furthermore, at the two-cell stage, following the first zygotic division, there was an even distribution of mitochondria between blastomeres. Due to the differences in staining patterns observed with the mitochondrial probes in embryos collected on day 3, we analyzed the 6- to 12-cell embryos separately from the 13- to 16-cell embryos. In 6- to 12-cell embryos, a clear compartmental distribution of mitochondria between the nucleus and the exterior membrane of the embryo in each blastomere was observed. In 16-cell embryos, there was a very limited number of mitochondria in the central blastomeres; many more mitochondria, with a specific compartmental distribution, were found in the external blastomeres. In addition, in 16-cell embryos, the staining intensity of mitochondria in the central blastomeres was extremely low compared with the high staining intensity in mitochondria located in the external blastomeres. The pattern of distribution of mitochondria was influenced by cell cycle phase in all cleavage-stage embryos; mitochondria in mitotic blastomeres lost their bean shape, were diffusely distributed in the whole cell, and stained less intensely than those in interphasic blastomeres (Fig. 1b). The specific localization of mitochondria in the blastomeres of cleavage-stage embryos may dictate the plan of cellular division with a concentration of

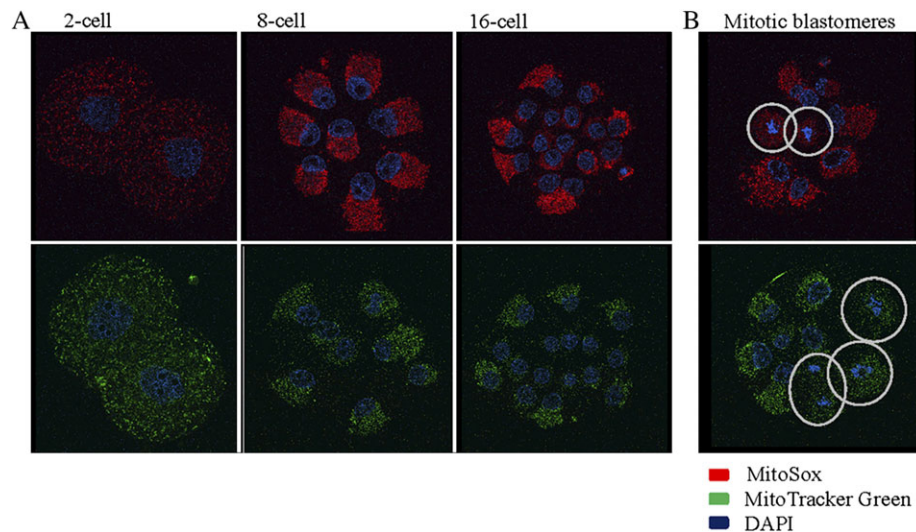


FIG. 1. Distribution of MitoTracker probes in cleavage-stage embryos. Immunodetection of active mitochondria by MitoSox red, indicated in red, and MitoTracker green, depicted in green, in 2-, 8-, and 16-cell embryos. (A) Even distribution of mitochondria in blastomeres of two-cell embryos compared with the stage-specific functional compartmentalization in eight-cell embryos. A faint low count of mitochondria was observed in central blastomeres compared with the specialized darker distribution of mitochondria in the external blastomeres of 16-cell embryos. (B) Cell cycle-dependent mitochondrial pattern of staining, mitotic blastomeres, circled in white, had a fainter diffuse pattern of staining, as opposed to the darker, specific distribution, in interphasic blastomeres.

all the energy producing organelles where they are most needed, thus playing a role in the cell fate decision.

Although quantification revealed a trend toward an increase in the mitochondrial mean intensity and a decrease in mitochondrial count per embryo from the two- to the eight-cell stage, these parameters were not significantly different between cleavage stages and treatment groups (Supplementary fig. 1a), nor did the presence of micronuclei within a cell influence our results with MitoTracker probes at any of the cell cleavage stages (Supplementary fig. 1b).

The Characterization of γ H2AX Foci in Control- and Cyclophosphamide-Sired Cleavage-Stage Embryos

To evaluate the level of DNA damage as a consequence of paternal exposure to cyclophosphamide in cleavage-stage embryos, we assessed the distribution pattern of γ H2AX signals (Fig. 2). In both control- and cyclophosphamide-sired two-cell embryos, γ H2AX foci were uniformly distributed, suggesting that these foci may be indicative of replication stress (Fig. 2, top two rows). The staining pattern with γ H2AX in embryos collected on day 3 did not differ in 8- and 16-cell embryos; therefore, we pooled these data and show only the eight-cell embryos. In the eight-cell embryos, γ H2AX foci appeared to be increased in size and be more irregularly distributed in embryos sired by cyclophosphamide-treated males compared with controls (Fig. 2, bottom two rows).

To further characterize the population of γ H2AX foci, we subdivided them into three subgroups, based on their volumes, and calculated the average number of each type of foci per nucleus (Fig. 3). Control- and cyclophosphamide-sired two-cell embryos had nearly four times as many foci as eight-cell stage embryos; paternal exposure to cyclophosphamide had no impact on the number of small foci at the two-cell and eight-cell stages (Fig. 3a, left panel). Although a similar decreasing trend, by just over 50%, in the number of medium-sized γ H2AX foci was observed between two- and eight-cell embryos in the control group, embryos sired by cyclophosphamide-treated males showed a steeper decline, and the numbers were more elevated than for control at the eight-cell stage ($p \leq 0.05$) (Fig. 3a, middle panel). In contrast to the decrease observed in small- and medium-sized foci between two- and eight-cell stage embryos, a significant increase was observed in the numbers of large γ H2AX foci in both treatment groups ($p \leq 0.05$) (Fig. 3a, right panel). Few large γ H2AX foci were observed in control- and cyclophosphamide-sired two-cell embryos. A dramatic increase in the number of large γ H2AX foci was observed in eight-cell embryos sired by cyclophosphamide-treated males compared with same stage control embryos ($p \leq 0.01$). The decrease in small and medium γ H2AX foci per nucleus between the two- and eight-cell embryos may reflect important events in preimplantation embryo development, such as the major and minor waves of transcription and active DNA replication in two- and four-cell embryos; the significant increase in the number of large γ H2AX foci in

eight-cell embryos sired by males treated with cyclophosphamide compared with control eight-cell embryos is likely to reflect an increase in the formation of DNA DSB aggregates.

Because the amount of DNA damage, represented by γ H2AX foci, depends on the nuclear volume to compare DNA damage in micronuclei to nuclei, we divided the number of foci by the average nuclear volume for the nucleus and by the average micronuclear volume for the micronucleus and report the fold differences for the relative values in two- and eight-cell embryos (Fig. 3b). The majority of micronuclei were punctuated with numerous γ H2AX foci. There were no differences between the nuclei and micronuclei in the numbers of small, medium, and large γ H2AX foci in two-cell embryos (Fig. 3b). However, in cyclophosphamide-sired eight-cell embryos, a 1.5-fold increase in the medium γ H2AX foci ($p \leq 0.001$) and a 45-fold increase in the large γ H2AX foci ($p \leq 0.001$) were observed in micronuclei compared with nuclei (Fig. 3b). Thus, medium ($p \leq 0.05$) and large foci ($p \leq 0.01$) accumulate in the micronuclei of cyclophosphamide-sired eight-cell embryos (Fig. 3c). This accumulation of damage marks may represent an increase in the formation of DNA DSBs or in the sites of replication errors or a failure to recruit the appropriate DNA repair proteins.

Because micronuclei represent visible signs of DNA damage in cyclophosphamide-sired embryos, we hypothesized that the DNA damage response would be elevated in embryos with micronuclei compared with those without. To test this hypothesis, we compared the number of γ H2AX foci in the nuclei of cyclophosphamide-sired two- and eight-cell embryos with and without micronuclei (Supplementary fig. 2). Strikingly, the number of γ H2AX foci within each subgroup, classified by their volume, was not dependent on the presence and/or abundance of micronuclei in the embryos; there was also no correlation between the nuclear DNA damage response in individual blastomeres and the presence or absence of micronuclei within the cell (Supplementary fig. 2a). Embryos fertilized by cyclophosphamide-exposed spermatozoa and collected on day 3 were considered developmentally delayed if they were at the three- and four-cell stage; normally dividing embryos, sired by control- or cyclophosphamide-treated males, were at the 5- to 16-cell stage at this time (Grenier *et al.*, 2011). Developmentally delayed cyclophosphamide-sired embryos, with the highest incidence of micronuclei, had the same DNA damage response profile, as assessed by the numbers of γ H2AX foci, as normally dividing embryos (Supplementary fig. 2b). Thus, the presence of micronuclei did not affect the numbers of γ H2AX foci in the nuclei of cells within cleavage-stage embryos.

53BP1 in Cleavage-Stage Embryos

Our next objective was to determine whether fertilization with cyclophosphamide-exposed spermatozoa would affect markers of DNA repair in cleavage-stage embryos. The localization of 53BP1 immunoreactivity in pronuclear, two- and eight-cell

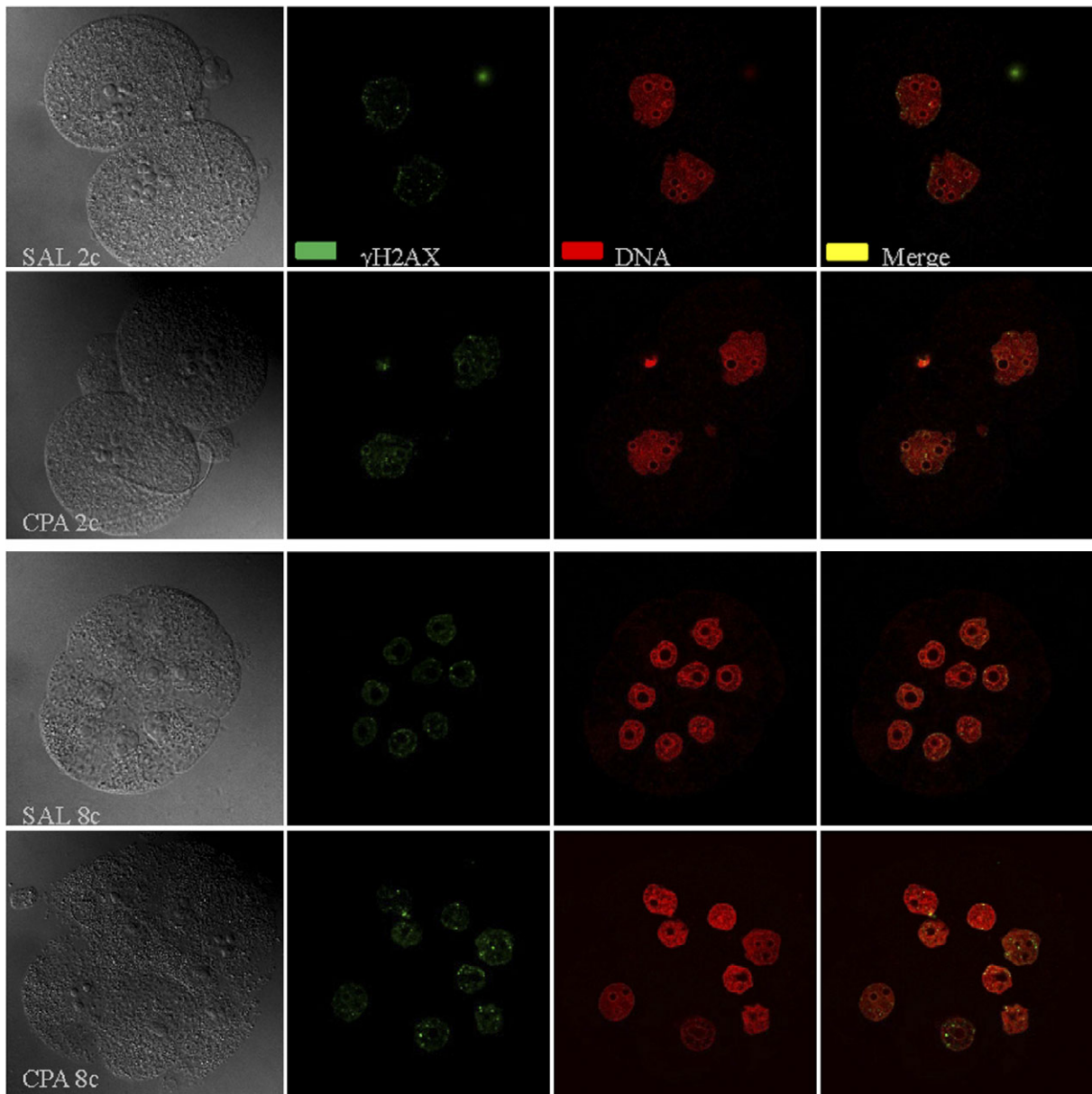


FIG. 2. γ H2AX detection of DNA DSBs in cleavage-stage embryos. The detection of DNA DSBs with γ H2AX in control- and cyclophosphamide-sired two- and eight-cell embryos. Phase-contrast images with immunodetection of γ H2AX in green, nuclear propidium iodide dye in red, and merged images in yellow. The top two rows are control- and cyclophosphamide-sired two-cell embryos, showing an even distribution of small γ H2AX foci. The bottom two rows are control- and cyclophosphamide-sired eight-cell embryos, showing nuclear region-specific large γ H2AX foci in the cyclophosphamide-sired eight-cell embryos compared with control.

embryos is depicted in Figure 4. The 53BP1 signal was distributed throughout the nucleus and cytoplasm. To determine the relative amounts of 53BP1 reactivity in these two compartments, we quantified the average intensities in the nucleus and the cytoplasm as well as the nuclear to cytoplasmic ratio in the female and male pronuclei of the two- and eight-cell embryos (Fig. 4b). Because intensities did not differ between the male and female pronuclei, the average nuclear staining intensity is given as a single value for the pronuclear-stage embryos (Fig. 4b, left

graph day 0.5, pronuclear stage embryos, PN). The staining pattern of 53BP1 in 8- to 16-cell embryos collected on day 3 was identical irrespective of the treatment group; therefore, we pooled these data and show only the eight-cell embryos. The nuclear staining tended to increase as the embryos progressed from the pronuclear stage to the 8-cell stage in both the control- and cyclophosphamide-sired groups (Fig. 4b, left graph); this was accompanied by a trend toward a decrease in the cytoplasmic 53BP1 signal (Fig. 4b, middle graph). Together,

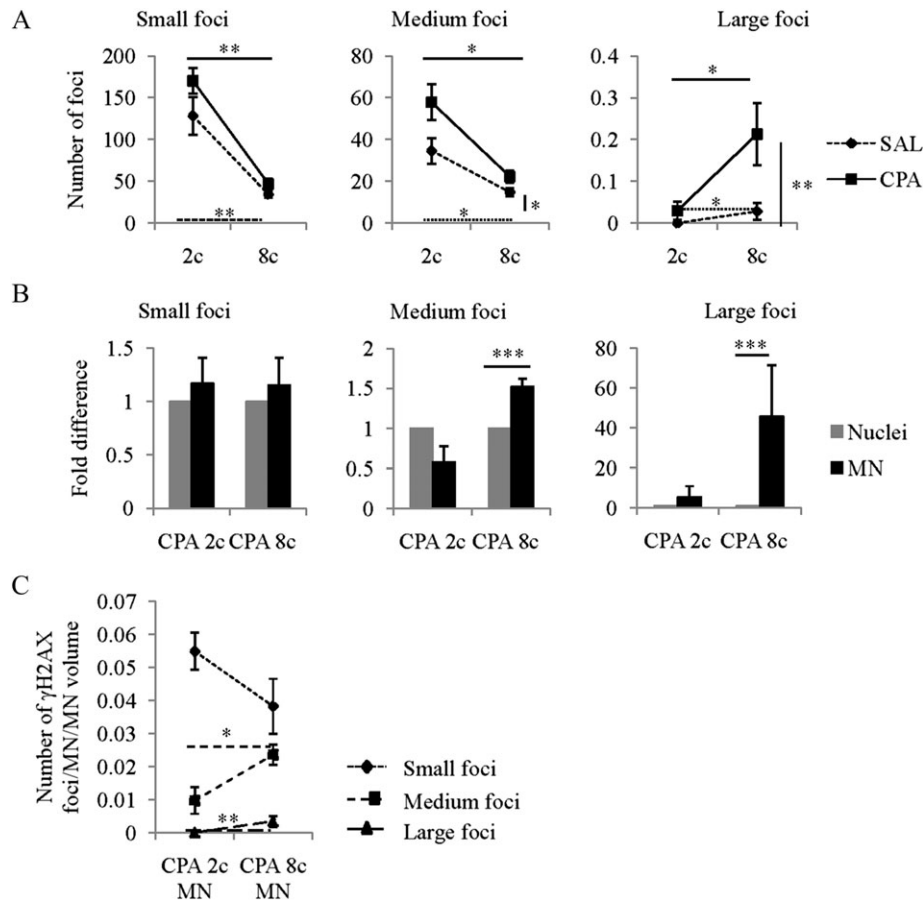


FIG. 3. Large γ H2AX foci as sites of DNA damage in cyclophosphamide-sired eight-cell embryos. The focal populations of γ H2AX foci were divided into three subgroups based on their volumes: Small foci, $0\text{--}0.29\ \mu\text{m}^3$; medium foci, $0.30\text{--}9.99\ \mu\text{m}^3$; and large foci, $10\ \mu\text{m}^3$ and above. The numbers of foci were quantified from immunofluorescence images of two- and eight-cell embryos. (A) Average numbers of foci per nucleus \pm SEM are graphed; dashed lines are control- and full lines are cyclophosphamide-sired embryos. There were significantly more medium and large γ H2AX foci in the cyclophosphamide-sired eight-cell embryos compared with control (medium foci: control or saline [SAL] 14.77 ± 1.97 vs. cyclophosphamide-sired, CPA, 22.96 ± 3.05 ; large foci: SAL 0.03 ± 0.02 vs. CPA 0.21 ± 0.07). (B) Comparison of the micronuclear with nuclear chromatin content of DNA DSBs in cyclophosphamide-sired cleavage-stage embryos with micronuclei (MN). Average number of small, medium, and large γ H2AX foci per micronucleus (MN) or nucleus corrected for their volume in two- and eight-cell embryos. Bar graphs represent the micronuclear fold difference from nuclei; micronuclear values are relative to the nuclear value set to $1 \pm$ SEM. Gray bars represent nuclei, and black bars are the MN. MN in cyclophosphamide-sired eight-cell embryos have 1.52- and 45.65-fold increases in the numbers of medium and large γ H2AX foci relative to their nuclear counterparts. (C) Changes in the numbers of γ H2AX foci in MN of cyclophosphamide-sired early cleavage-stage embryos. Line graphs represent the average number of γ H2AX foci, within their respective groups, per MN corrected for micronuclear volume \pm SEM. Illustrated in the figure legend, small, medium, and large dashed lines represent the sizes of the γ H2AX foci, respectively. MN significantly accumulated medium ($0.009\text{--}0.024$) and large ($0.000\text{--}0.003$) γ H2AX foci in cyclophosphamide-sired two- and eight-cell embryos. Mann-Whitney U -test was performed with $N = 7$, 10 males with 64, 99 embryos in control and $N = 5$, 7 males with 41, 112 embryos in cyclophosphamide-sired in two- and eight-cell embryos, respectively. $*p \leq 0.05$, $**p \leq 0.01$, and $***p \leq 0.001$.

these changes resulted in a significant increase in the nuclear to cytoplasmic ratio of the localization of the 53BP1 signal from the pronuclear-stage to the 8-cell embryo in both the control- ($0.84\text{--}1.74$, $p \leq 0.01$) and the cyclophosphamide-treated group ($0.85\text{--}1.45$, $p \leq 0.05$) (Fig. 4b, right graph).

To characterize DNA repair capacity in the chromatin of micronuclei found in cyclophosphamide-sired embryos, we compared the intensity of 53BP1 reactivity in the micronuclei with that in the nuclei. The 53BP1 intensities in the micronuclei and nuclei were adjusted by the ratios of DNA intensity because micronuclei have less DNA per equivalent

volume. In both the two- and eight-cell cyclophosphamide-sired embryos, the micronuclear chromatin contained significantly more 53BP1 repair protein (1.4-fold in two-cell, $p \leq 0.05$; 1.2-fold in eight-cell, $p \leq 0.01$) compared with the nuclear chromatin (Fig. 4c). Thus, this repair protein is actively recruited to micronuclear chromatin.

Similar to the number of γ H2AX foci, 53BP1 nuclear reactivity was not affected by the presence and/or abundance of micronuclei in the embryos; there was also no correlation between the nuclear DNA damage response in individual blastomeres and the presence or absence of micronuclei within

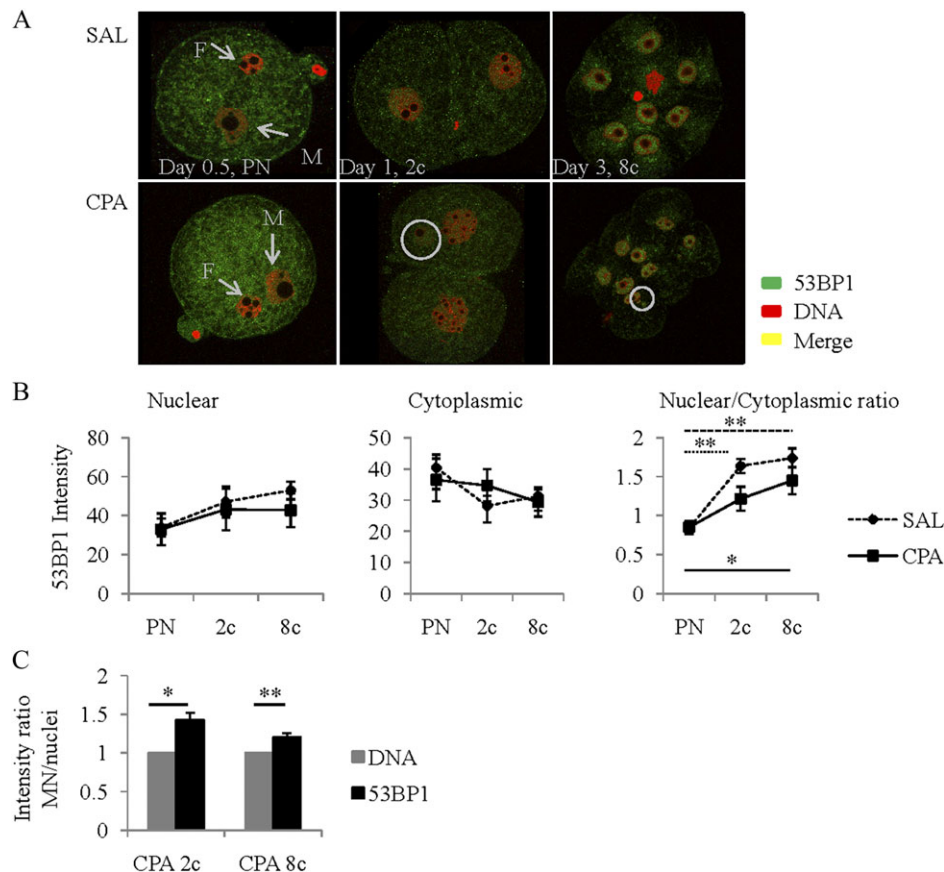


FIG. 4. 53BP1 reactivity in cleavage-stage embryos. (A) 53BP1 reactivity in pronuclear zygotes, two- and eight-cell embryos from control- and cyclophosphamide-sired groups. 53BP1 is in green, nuclear propidium iodide dye in red, and merged images in yellow. The top row images are control embryos, whereas bottom row images are cyclophosphamide-sired embryos at all embryonic cleavage stages. Arrows point toward the female (F) and male (M) pronuclei (PN) and the micronuclei (MN) as circled in white. (B) Immunofluorescence images are quantified as the 53BP1 intensity in the nucleus, the cytoplasm and the ratio of the nucleus to cytoplasm as means \pm SEM. Dashed lines represent control- and full lines cyclophosphamide-sired embryos. Independent of treatment group, there was a cytoplasmic to nuclear shift in the localization of 53BP1 repair protein as the cleavage-stage embryo divided (SAL PN 0.84 ± 0.06 ; SAL 8c 1.74 ± 0.12 ; CPA PN 0.85 ± 0.09 ; and CPA 8c 1.45 ± 0.17). C. Comparison of the micronuclear with nuclear chromatin content of 53BP1 repair protein in cyclophosphamide-sired cleavage-stage embryos with MN. Bar graphs illustrate the 53BP1 reactivity fold difference between their micronuclear and nuclear counterparts, comparing the relative micronuclear with nuclear average 53BP1 intensity mean ratios with DNA intensity ratios, both set to $1 \pm$ SEM. Gray bars are the DNA ratios, and black bars are the 53BP1 intensity ratios. In two- and eight-cell embryos, MN are enriched with 53BP1 repair proteins (1.43- and 1.20-fold increases in cyclophosphamide-sired two- and eight-cell embryos), relative to the nuclei. Kruskal-Wallis analysis plus Bonferroni's correction, when needed, was performed with $N = 6-8$ males with 57-63 embryos in the control group and $N = 4-7$ males with 32-68 embryos in the cyclophosphamide-sired group. Comparisons of the intensity means using the Mann-Whitney U -test was performed with $N = 4-6$ males with 24-45 embryos for the micronuclei to nuclei comparison. * $p \leq 0.05$, ** $p \leq 0.01$, and *** $p \leq 0.001$.

the cell (Supplementary fig. 3a). In addition, developmentally delayed cyclophosphamide-sired embryos had the same DNA damage response profile, assessed by the nuclear reactivity with 53BP1, as normally dividing embryos (Supplementary fig. 3b).

Poly(ADP-ribose) Polymers in Cleavage-Stage Embryos

The immunoreactive poly(ADP-ribose) polymers (PAR), representing the product of poly(ADP-ribose) polymerase activities, in pronuclear two- and eight-cell embryos are shown in Figure 5a. The PAR signal was consistently more intense in the nucleus compared with the cytoplasm. As for 53BP1, the PAR immunoreactivity did not differ between the male and female pronuclei of pronuclear-stage embryos. The

staining pattern also did not differ between 8- and 16-cell embryos irrespective of the treatment group. Neither developmental stage nor treatment significantly affected the intensity of the PAR signal in the cytoplasm or the nuclear to cytoplasmic ratio (Fig. 5b, middle and right graph). In contrast, embryos sired by cyclophosphamide-treated males displayed a dramatic decrease in PAR nuclear mean intensity at the eight-cell cleavage stage ($p \leq 0.01$) (Fig. 5b, left graph). In both the two- and eight-cell cyclophosphamide-sired embryos, the micronuclear chromatin contained significantly more PAR polymers (1.5-fold in two-cell, $p \leq 0.01$; 1.3-fold in eight-cell, $p \leq 0.01$) compared with the nuclear chromatin (Fig. 5c).

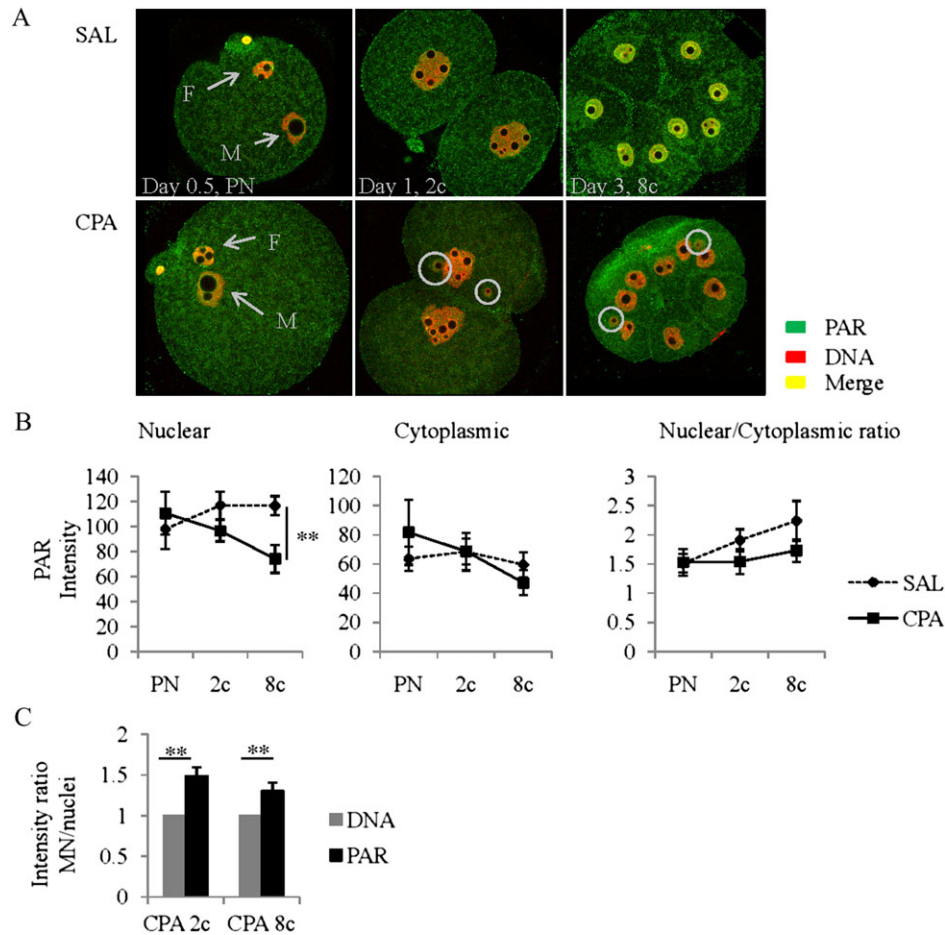


FIG. 5. Poly(ADP-ribose) (PAR) polymer reactivity in cleavage-stage embryos. (A) Poly(ADP-ribose) polymer (PAR) reactivity in pronuclear zygotes, two- and eight-cell control- and cyclophosphamide-sired embryos. PAR is in green, nuclear propidium iodide dye in red, and merged images in yellow. The top row images are control embryos, whereas the bottom row images are cyclophosphamide-sired embryos at all embryonic cleavage stages. Arrows point toward the female (F) and male (M) pronucleus (PN) and micronuclei (MN) are circled in white. (B) Immunofluorescence images are quantified into nuclear, cytoplasmic, and nuclear to cytoplasmic ratios of PAR intensity means \pm SEM. Dashed lines are control- and full lines are cyclophosphamide-sired embryos. There is a significant decrease in the nuclear PAR reactivity in cyclophosphamide-sired embryos at the eight-cell stage compared with control embryos (SAL 8c is 116.68 ± 7.67 vs. cyclophosphamide 8c at 74.17 ± 11.19). (C) Comparison of the micronuclear with nuclear chromatin content of PAR polymer reactivity in cyclophosphamide-sired cleavage-stage embryos with MN. Bar graphs illustrate the micronuclear fold difference in PAR reactivity from their nuclear counterpart by comparing the relative micronuclear with nuclear average PAR intensity mean ratios with the DNA intensity ratios, both set to $1 \pm$ SEM. Gray bars are the DNA ratios, and black bars are the PAR ratios. In two- and eight-cell embryos, MN are enriched with PAR polymers (1.49- and 1.30-fold increase in cyclophosphamide-sired two- and eight-cell embryos) relative to the nuclei. Kruskal-Wallis analysis plus Bonferroni's correction, when necessary, was performed, $N = 6-8$ males with 51-72 embryos in control and $N = 4-6$ males with 34-52 embryos in the cyclophosphamide-sired group for the PAR localization and intensity means. The Mann-Whitney U -test was performed with $N = 5-6$ males with 23-37 embryos for the micronuclear to nuclear comparison. $*p \leq 0.05$, $**p \leq 0.01$, and $***p \leq 0.001$.

Once again, the nuclear signal of PAR polymers was not affected by the presence and/or abundance of micronuclei in the two- and eight-cell cyclophosphamide-sired embryos (Supplementary fig. 4a) or, in eight-cell cyclophosphamide-sired embryos, by a delay in the rate of development (Supplementary fig. 4b).

DISCUSSION

Paternal exposure to cyclophosphamide did not affect mitochondrial functional compartmentalization or bioenergetic activities in cleavage-stage embryos. However, markers of the

DNA damage detection and repair responses were affected. In the eight-cell embryo, paternal cyclophosphamide exposure led to the selective formation of medium and large γ H2AX foci and a decrease in nuclear PAR polymers in the absence of an effect on 53BP1 reactivity. All three DNA damage response indicators were enriched in micronuclei. However, cells with micronuclei had a similar DNA damage response to those without micronuclei.

The specialized localization of mitochondria during embryonic development is hypothesized to play a critical role in the regulation of energy production and consumption as well as roles in calcium homeostasis, cytoplasmic redox state, and

signal transduction (van Blerkom, 2011). As observed for human and mouse embryos (van Blerkom, 2011), the staining intensities and distribution patterns of MitoTracker green and MitoSox red in early embryos display embryonic developmental stage and compartmental specificity. In eight-cell embryos, the localization of mitochondria between the nucleus and the plasma membrane on a specific side of the embryo may determine the plane of the next cycle of division by concentrating the energy necessary to allow normal developmental progression. In 16-cell embryos, we observed a very faint diffuse type of staining for mitochondria in central blastomeres, as opposed to a stronger and compartmentalized type of staining in blastomeres surrounding the embryo. These stage- and space-specific mitochondrial distributions closely resemble the differences in mitochondrial structure and number between the two cell types in the future blastocyst; inner cell mass cells are hypopolarized, almost metabolically quiescent, as opposed to the trophectoderm cells that are hyperpolarized at the basal aspect of the plasma membrane and produce almost 80% of the net ATP (Houghton, 2006; van Blerkom *et al.*, 2002). Because the initial pool of mitochondria in the oocyte is not replenished until after blastocyst implantation and mitochondria are evenly divided between blastomeres, there was a tendency for the mitochondrial count per blastomere to decrease as the embryos progressed through cleavage stages (Larsson *et al.*, 1998).

If fertilization with cyclophosphamide-exposed spermatozoa had increased energy demand in the embryo due to the requirement for an enhanced DNA repair response, we might have anticipated a decrease in energy stores. However, fertilization with cyclophosphamide-exposed spermatozoa did not have any impact on the distribution or staining intensity of the mitochondrial MitoTracker Green or MitoSox Red probes, indicating that the general energy stores and intracellular redox status of cleavage-stage embryos were unaltered. Thus, the MitoSox and MitoTracker probes were valuable tools to show that embryos with damaged DNA may be otherwise normal, at least in terms of energy stores. It is clear that the mitochondrial energetic status observed in early cleavage-stage embryos is sufficient to allow the progression of embryos during pre-implantation development even in the presence of heavy DNA damage. Moreover, these results indicate that mitochondrial function is not, by itself, sufficient to predict development competence, especially for male-mediated DNA damage such as that induced by cyclophosphamide.

In cleavage-stage embryos, we observed the greatest level of H2AX phosphorylation at the two-cell stage, coincident with major chromatin reorganization during DNA replication and zygotic genome activation; the level of staining was significantly reduced at the eight-cell stage. H2AX is phosphorylated in response to DNA DSBs that arise from exposure to exogenous chemicals, radiation or reactive oxygen species that induce replication stress (Ismail *et al.*, 2007; Rogakou *et al.*, 1998), as well as in response to physiological processes,

such as DNA replication errors, chromatin remodeling during protamine to histone transition in pre-pronuclear zygotes, and meiosis (Grenier *et al.*, 2010). The small γ H2AX foci observed support a role for the phosphorylation of H2AX in the control of chromatin structural reorganization (Barton *et al.*, 2007) and proper developmental progression of rapidly dividing stressed embryos (Ziegler-Birling *et al.*, 2009) in the absence of induced DNA damage. The significant increase in medium γ H2AX foci in cyclophosphamide-sired eight-cell embryos, compared with controls, suggests that these medium foci may be important in the recognition of DNA damage. The large γ H2AX foci visualized in eight-cell embryos sired by cyclophosphamide-treated males are likely to represent the accumulation of γ H2AX at hot spots of DNA damage, perhaps as a consequence of the failure to complete the repair process in early embryos (Barton *et al.*, 2007; Grenier *et al.*, 2010). Earlier studies have reported a similar phenomenon in a murine model; paternal exposure to radiation impaired blastocyst development due to inappropriate repair during the first cell cycle division and led to *de novo* mutations (Derijck *et al.*, 2008). Interestingly, the presence of micronuclei in early embryos did not influence the quantity or nature of the γ H2AX foci in the nuclei of these embryos.

DNA damage repair capacity in cleavage-stage embryos was assessed in the pronuclear zygote, two- and eight-cell embryo with two markers of DNA repair, 53BP1 and poly(ADP-ribose) polymers, that are known to be recruited to the sites of DNA DSBs detected by γ H2AX. It is not likely that the 53BP1 immunoreactivity is strongly colocalized with γ H2AX in these embryos because a faint diffuse and homogenous pattern of 53BP1 distribution was observed in both the nuclear and cytoplasmic compartments throughout the cell cleavage stages studied. In addition, 53BP1 protein expression was unaffected by the presence of a damaged male genome. Similar findings were reported previously in a damage free mouse embryonic model in which 53BP1 protein localization changed upon blastocyst formation. The failure of 53BP1 and γ H2AX to colocalize in the embryo (Ziegler-Birling *et al.*, 2009) reinforces the notion that the high levels of H2AX phosphorylation may be linked to chromatin remodeling in the early embryo rather than directly to a DNA damage response (Ziegler-Birling *et al.*, 2009). The developmental significance of the nuclear retention of 53BP1 as a partial mediator of p53 activity in regulating cell cycle checkpoints, allowing the progression of cell cycle division of cleavage-stage embryos, has been established previously (Fernandez-Capetillo *et al.*, 2003).

A decrease in nuclear poly(ADP-ribose) polymers was observed in eight-cell embryos sired by cyclophosphamide-exposed spermatozoa. The presence of micronuclei did not influence the amount of poly(ADP-ribose) polymers in the nucleus. In general, a decrease in poly(ADP-ribose) polymers is suggestive of a decrease in the poly(ADP-ribosylation) of histones and/or PARP-1 (Zhou *et al.*, 2010). This may result in

the recondensation of chromatin, reducing the accessibility of potential DNA damage repair proteins to DNA (Zhou *et al.*, 2010); however, examination of the gross nuclear morphology of cyclophosphamide-sired eight-cell embryos did not reveal any apparent increase in condensed chromatin. Numerous scenarios could lead to a decrease in poly(ADP-ribosylation) in early embryos; these include NADH energy depletion, reducing PARP-1 activity, an increase in PARP-1 activity, leading to auto-poly(ADP-ribosylation) of PARP-1 and its inactivation, or an increase in PARG catalytic activity, removing poly(ADP-ribose) polymers. Previously, we reported that paternal exposure to cyclophosphamide led to an increase in PARP-1 immunoreactivity in both male and female pronuclei (Barton *et al.*, 2007). Our data show that there is no drug treatment effect on the level of poly(ADP-ribosylation) in pronuclear or two-cell embryos, suggesting that the increase in PARP-1 immunoreactivity may be accompanied by an increase in PARG catalytic activity, dampening the repair capacity of cleavage-stage embryos. The reduced PARP-1 activity observed in eight-cell embryos was not associated with a decrease in mitochondrial energy status, as assessed with the MitoTracker probes; therefore, the reduction in PAR polymers does not appear to be due to a decrease in energy stores in the embryo.

Energy depletion as a result of PARP-induced NADH depletion may contribute to the delay in cell cycle progression seen at the eight-cell stage (Grenier *et al.*, 2011). Developmental arrest was reported in pronuclear-stage mouse embryos treated with a PARP inhibitor (Osada *et al.*, 2010). It is clear that the proper functioning of the complex poly(ADP-ribosylation) system is necessary for the early stages of mouse embryogenesis (Osada *et al.*, 2010).

Micronuclei are a readily identifiable mark of DNA damage in the paternal genome in embryos sired by cyclophosphamide-treated males. In two- and eight-cell embryos, both 53BP1 and poly(ADP-ribose) polymers were enriched in chromatin in the micronuclei compared with the nuclei; this enrichment was observed in the absence of any increase in γ H2AX foci, tagging DNA DSBs. These findings suggest that there may be a γ H2AX-independent mechanism of recruitment of 53BP1 and poly(ADP-ribose) polymers in micronuclei at the two-cell stage. By the eight-cell stage, a marked accumulation of medium and large γ H2AX foci was observed in micronuclei; this occurred in the absence of an increase in the intensity of the staining for 53BP1 or poly(ADP-ribose) polymers in comparison with the two-cell embryos. The accumulation of γ H2AX foci in the micronuclei of eight-cell embryos may indicate the failure of DNA repair processes to resolve DNA DSBs (Celeste *et al.*, 2003). Micronuclei may gradually lose functionality as the embryo progresses from two-cells to eight-cells; indeed, we reported previously that the incorporation of EdU (5-ethynyl-2'-deoxyuridine) into DNA was decreased in micronuclei at the eight-cell stage (Grenier *et al.*, 2011).

In summary, we have demonstrated that fertilization by sperm from cyclophosphamide-treated male rats produces a conceptus with a heavily damaged paternal genome. The damaged paternal genome triggers both a γ H2AX-dependent and a γ H2AX-independent DNA damage response with respect to micronuclear formation, within the same cells. The two-cell embryo is capable of mounting a DNA damage response because there is a recruitment of 53BP1 and an increase in poly(ADP-ribose) polymers in micronuclei. However, the DNA repair response is not adequate to prevent the accumulation of medium and large γ H2AX foci in micronuclei by the eight-cell stage. The accumulation of DNA damage and the inability of the embryo to adequately repair the paternal genome are likely to contribute to the elevated pre- and postimplantation death observed as a consequence of paternal cyclophosphamide exposure.

SUPPLEMENTARY DATA

Supplementary data are available online at <http://toxsci.oxfordjournals.org/>.

FUNDING

Canadian Institutes of Health Research (MOP-14851).

ACKNOWLEDGMENTS

We thank Jacynthe Laliberté (McGill University, Montreal) for her assistance with confocal microscopy and Aleksandrs Spurmanis and Claire Brown (McGill University, Montreal) and Cory Glowinski (Bitplane Inc.) for their assistance with Imaris image analysis.

REFERENCES

- Auroux, M., Dulioust, E., Selva, J., and Rince, P. (1990). Cyclophosphamide in the F0 male rat: Physical and behavioral changes in three successive adult generations. *Mutat. Res.* **229**, 189–200.
- Barton, T. S., Robaire, B., and Hales, B. F. (2005). Epigenetic programming in the preimplantation rat embryo is disrupted by chronic paternal cyclophosphamide exposure. *Proc. Natl. Acad. Sci. U.S.A.* **31**, 7865–7870.
- Barton, T. S., Robaire, B., and Hales, B. F. (2007). DNA damage recognition in the rat zygote following chronic paternal cyclophosphamide exposure. *Toxicol. Sci.* **100**, 495–503.
- Barton, T. S., Wyrobek, A. J., Hill, F. S., Robaire, B., and Hales, B. F. (2003). Numerical chromosomal abnormalities in rat epididymal spermatozoa following chronic cyclophosphamide exposure. *Biol. Reprod.* **69**, 1150–1157.
- Brochu, G., Duchaine, C., Thibeault, L., Lagueux, J., Shah, G. M., and Poirier, G. G. (1994). Mode of action of poly(ADP-ribose) glycohydrolase. *Biochim. Biophys. Acta* **1219**, 342–350.
- Celeste, A., Fernandez-Capetillo, O., Kruhlak, M. J., Pilch, D. R., Staudt, D. W., Lee, A., Bonner, R. F., Bonner, W. M., and Nussenzweig, A. (2003). Histone H2AX phosphorylation is dispensable for the initial recognition of DNA breaks. *Nat. Cell Biol.* **5**, 675–679.

- Codrington, A. M., Hales, B. F., and Robaire, B. (2004). Spermio-genic germ cell phase-specific DNA damage following cyclophosphamide exposure. *J. Androl.* **25**, 354–362.
- Codrington, A. M., Hales, B. F., and Robaire, B. (2007a). Chronic cyclophosphamide exposure alters the profile of rat sperm nuclear matrix proteins. *Biol. Reprod.* **77**, 303–311.
- Codrington, A. M., Hales, B. F., and Robaire, B. (2007b). Exposure of male rats to cyclophosphamide alters the chromatin structure and basic proteome in spermatozoa. *Hum. Reprod.* **22**, 1431–1442.
- D'Amours, D., Desnoyers, S., D'Silva, I., and Poirier, G. G. (1999). Poly(ADP-ribose)ylation reactions in the regulation of nuclear functions. *Biochem. J.* **342**(Part 2), 249–268.
- Dantzer, F., Schreiber, V., Niedergang, C., Trucco, C., Flatter, E., De La Rubia, G., Oliver, J., Rolli, V., Meissier-de Murcia, J., and de Murcia, G. (1999). Involvement of poly(ADP-ribose) polymerase in base excision repair. *Biochimie* **81**, 69–75.
- Derijck, A., van der Heijden, G., Giele, M., Philippens, M., and de Boer, P. (2008). DNA double-strand break repair in parental chromatin of mouse zygotes, the first cell cycle as an origin of de novo mutation. *Hum. Mol. Genet.* **17**, 1922–1937.
- Fernandez-Capetillo, O., Chen, H. T., Celeste, A., Ward, I., Romanenko, P. J., Morales, J. C., Naka, K., Xia, Z., Camerini-Otero, R. D., Motoyama, N., et al. (2003). DNA damage-induced G2-M checkpoint activation by histone H2AX and 53BP1. *Nat. Cell Biol.* **4**, 993–997.
- Green, D. M., Kawashima, T., Stovall, M., Leisenring, W., Sklar, C. A., Mertens, A. C., Donaldson, S. S., Byrne, J., and Robison, L. L. (2010). Fertility of male survivors of childhood cancer: A report from the childhood cancer survivor study. *J. Clin. Oncol.* **28**, 332–339.
- Grenier, L., Robaire, B., and Hales, B. F. (2010). Paternal exposure to cyclophosphamide affects the progression of sperm chromatin decondensation and activates a DNA damage response in the prepronuclear rat zygote. *Biol. Reprod.* **83**, 195–204.
- Grenier, L., Robaire, B., and Hales, B. F. (2011). Paternal cyclophosphamide exposure induces the formation of functional micronuclei during the first zygotic division. *PLoS One* **6**, e27600.
- Hales, B. F., Crosman, K., and Robaire, B. (1992). Increased postimplantation loss and malformations among the F2 progeny of male rats chronically treated with cyclophosphamide. *Teratology* **45**, 671–678.
- Houghton, F. (2006). Energy metabolism of the inner cell mass and trophectoderm of the mouse blastocyst. *Differentiation* **74**, 11–18.
- Ismail, I. H., Wadhwa, T. I., and Hammarsten, O. (2007). An optimized method for detecting gamma-H2AX in blood cells reveals a significant interindividual variation in the gamma-H2AX response among humans. *Nucleic Acids Res.* **35**, e36.
- Iwabuchi, K., Li, B., Massa, H. F., Trask, B. J., Date, T., and Fields, S. (1998). Stimulation of p53-mediated transcriptional activation by the p53-binding proteins, 53BP1 and 53BP2. *J. Biol. Chem.* **273**, 26061–26068.
- Kim, M. Y., Mauro, S., Gevry, N., Lis, J. T., and Kraus, W. L. (2004). NAD⁺-dependent modulation of chromatin structure and transcription by nucleosome binding properties of PARP-1. *Cell* **119**, 803–814.
- Larsson, N., Wang, J., Wilhelmsson, H., Oldfors, A., Rustin, P., Lewandoski, M., Barsh, G., and Clayton, D. (1998). Mitochondria transcription factor A is necessary for mtDNA maintenance and embryogenesis in mice. *Nat. Genet.* **18**, 231–236.
- Marchetti, F., Essers, J., Kanaar, R., and Wyrobek, A. J. (2007). Disruption of maternal DNA repair increases sperm-derived chromosomal aberrations. *Proc. Natl. Acad. Sci. U.S.A.* **104**, 17725–17729.
- McManus, K. J., and Hendzel, M. J. (2005). ATM-dependent DNA damage-independent mitotic phosphorylation of H2AX in normally growing mammalian cells. *Mol. Biol. Cell* **16**, 5013–5025.
- Moudry, P., Lukas, C., Macurek, L., Neumann, B., Heriche, J. K., Pepperkok, R., Ellenberg, J., Hodny, Z., Lukas, J., and Bartek, J. (2011). Nucleoporin NUP153 guards genome integrity by promoting nuclear import of 53BP1. *Cell Death Differ.* **19**, 798–807.
- Oh, S. H., Miyoshi, K., and Funahashi, H. (1998). Rat oocytes fertilized in modified rat 1-cell embryo culture medium containing a high sodium chloride concentration and bovine serum albumin maintain developmental ability to the blastocyst stage. *Biol. Reprod.* **59**, 884–889.
- Osada, T., Ogino, H., Hino, T., Ichinose, S., Nakamura, K., Omori, A., Noce, T., and Masutani, M. (2010). PolyADP-ribosylation is required for pronuclear fusion during postfertilization in mice. *PLoS One* **5**, pii:e12526.
- Paull, T. T., Rogakou, E. P., Yamazaki, V., Kirchgessner, C. U., Gellert, M., and Bonner, W. M. (2000). A critical role for histone H2AX in recruitment of repair factors to nuclear foci after DNA damage. *Curr. Biol.* **10**, 886–895.
- Rogakou, E. P., Pilch, D. R., Orr, A. H., Ivanova, V. S., and Bonner, W. M. (1998). DNA double-stranded breaks induce histone H2AX phosphorylation on serine 139. *J. Biol. Chem.* **273**, 5858–5868.
- Schreiber, V., Dantzer, F., Ame, J. C., and de Murcia, G. (2006). Poly(ADP-ribose): Novel functions for an old molecule. *Nat. Rev. Mol. Cell Biol.* **7**, 517–528.
- Trasler, J. M., Hales, B. F., and Robaire, B. (1986). Chronic low dose cyclophosphamide treatment of adult male rats: Effect on fertility, pregnancy outcome and progeny. *Biol. Reprod.* **34**, 275–283.
- van Blerkom, J. (2011). Mitochondrial function in the human oocyte and embryo and their role in developmental competence. *Mitochondrion* **11**, 797–813.
- van Blerkom, J., Davis, P., Mawhig, V., and Alexander, S. (2002). Domains of high and low polarized mitochondria in mouse and human oocytes and early embryos. *Hum. Reprod.* **17**, 393–406.
- Wang, B., Matsuoka, S., Carpentier, P. B., and Elledge, S. J. (2002). 53BP1, a mediator of the DNA damage checkpoint. *Science* **298**, 1435–1438.
- Ward, I. M., Minn, K., Van Deursen, J., and Chen, J. (2003). P53 binding protein 53BP1 is required for DNA damage responses and tumor suppression in mice. *Mol. Cell Biol.* **23**, 2556–2563.
- Ward, W. S. (2010). Function of sperm chromatin structural elements in fertilization and development. *Mol. Hum. Reprod.* **16**, 30–36.
- Yu, S. W., Wang, H., Poitras, M. F., Coombs, C., Bowers, W. J., Federoff, H. J., Poirier, G. G., Dawson, T. M., and Dawson, V. L. (2002). Mediation of poly(ADP-ribose) polymerase-1-dependent cell death by apoptosis-inducing factor. *Science* **297**, 259–263.
- Zhou, Y., Feng, X., and Koh, D. W. (2010). Enhanced DNA accessibility and increased DNA damage induced by the absence of poly(ADP-ribose) hydrolysis. *Biochemistry* **49**, 7360–7366.
- Ziegler-Birling, C., Helmrich, A., Tora, L., and Torres-Padilla, M. E. (2009). Distribution of p53 binding protein 1 (53BP1) and phosphorylated H2A.X during mouse preimplantation development in the absence of DNA damage. *Int. J. Dev. Biol.* **53**, 1003–1011.